ACS APPLIED ENERGY MATERIALS

www.acsaem.org Article

Electrochemical Hydrogen Storage under Ambient Conditions in Aqueous-Soluble Organics

Taobo Wang,[†] Dawei Xi,[†] and Michael J. Aziz*

Cite This: https://doi.org/10.1021/acsaem.4c01233 Read Online

ACCESS | Metrics & More | Article Recommendations | Supporting Information

ABSTRACT: We demonstrate and characterize a reversible aqueous low-voltage electrochemical flow cell for stationary hydrogen storage operating at ambient temperature and pressure and driven by a voltage swing of ≤800 mV. Hydrogen is stored by reversibly binding to anthraquinone disulfonate during electrochemical reduction and released during oxidation of the resulting hydroquinone molecule. The Faradaic efficiency is indistinguishable from 100%, and the round-trip energy cost of storage and release ranges from 1.6 to 12.5 kWh/kgH_2, with Coulombic efficiency ranging from 98.7 to 90.1%, as the current density ranges from 40 to 200 mA/cm^2. We show how the system can also be used for decoupled water splitting, which makes it possible for on-demand hydrogen release.

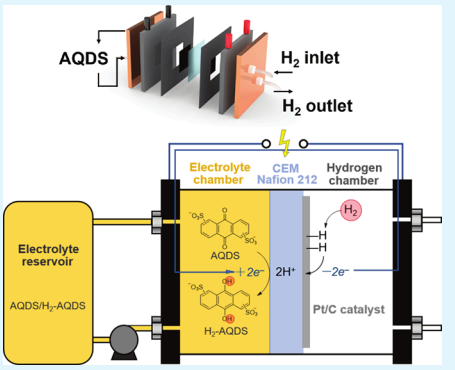

KEYWORDS: *electrochemistry, chemical engineering, hydrogen storage, flow battery, anthraquinone disulfonate, renewable energy*

INTRODUCTION

Hydrogen, which can be produced in an emission-free manner such as electrolysis is the focus of significant research and development due to its potential as an energy carrier in a low-emissions economy. Not only does hydrogen produce water as its combustion product, which has minimal environmental impact, but it also has the highest combustion energy per mass among all chemical fuels at about 40 kWh/kgH_2. This energy can be released as heat through direct combustion or as electricity through fuel cells. In addition to its high specific energy density, hydrogen has many other uses, including the electrochemical or thermochemical conversion of captured CO_2 to valuable chemicals and hydrocarbon fuels. Many envision a "hydrogen economy" in which hydrogen is widely used for various purposes.

Most industrial and utility consumers of natural gas, if they seek to suppress CO_2 emissions by replacing natural gas combustion with green hydrogen that is obtained by water electrolysis powered by wind or photovoltaics, require around-the-clock supplies of fuel for effective operation. Thus, the intermittency of these renewable energy sources necessitates either electricity or hydrogen storage.

One of the major challenges in enabling a hydrogen economy is safe and cost-effective stationary hydrogen storage. To date, state-of-the-art hydrogen storage materials have not been able to surpass the volumetric storage density of high-pressure compressed hydrogen for use in onboard vehicles.[1] Performance requirements for stationary applications, however, differ significantly from those for onboard vehicle applications. For example, the weight and volume constraints required for onboard storage can be relaxed for other use cases. These attributes can be traded off for facile, stable, and guaranteed safe storage in large quantities for long durations at low cost as well as the ability to be transported and transferred more easily.

Safe, stable containment of hydrogen gas is challenging due to its high diffusivity through plastics and many metals, which can cause metal embrittlement and lead to tank leakage or material failure. In addition, even without ignition, high-pressure hydrogen leakage can cause spontaneous combustion and explosion, as has been the case in accidents involving fuel tanks, refueling stations, and power plants.[2,3] Fatal explosions can occur during both large-scale hydrogen storage and transportation, highlighting the safety concerns associated with hydrogen usage.[4]

There are two main types of hydrogen storage techniques: direct and mediated storage. In direct storage, hydrogen is stored in its natural H_2 chemical form, e.g., as compressed gas, liquid hydrogen, and cryo-compressed hydrogen. For gas compression, which is the most commonly used method,[5] aluminum alloy tanks can hold only 30 bar of H_2, whereas high-pressure tanks up to 700 bar use composite materials.[5,6]

Received: May 13, 2024
Revised: July 11, 2024
Accepted: July 15, 2024

https://doi.org/10.1021/acsaem.4c01233
ACS Appl. Energy Mater. XXXX, XXX, XXX−XXX

The pressurization process requires 13−18% of the lower heating value (LHV) of hydrogen to reach 700 bar.[7,8] Liquid and cryo-compressed hydrogen not only have higher volumetric density[5] but also have substantial energy loss due to the liquefaction process (~30 to 40% LHV[6]) and high boil-off rate (1.5−3% per day[8]). Moreover, liquid or cryo-compressed hydrogen needs to be stored at cryogenic temperatures ~20 K.[6]

Mediated storage involves storing hydrogen with supporting compounds, such as porous host agents,[9] metal hydrides,[8] and organic molecules.[10] These methods can be classified into solid-state- and liquid-state mediated storage. Solid-state storage includes physisorption and chemisorption processes, but both have cost[11] and operational environment issues. These issues are related to the H_2 affinity enthalpies: physisorption has a low affinity enthalpy of −5 kJ/mol, meaning that the enthalpy decreases minimally upon physisorption. It is fully reversible at room temperature; therefore, it requires low temperature (i.e., ~77K) and high pressure (i.e., ~100 bar) for stable high-density storage.[11] In contrast, chemisorption has a high affinity enthalpy of approximately −75 kJ/mol, implying the need for high temperature for hydrogen release.[12] Liquid-state mediated storage employs liquid organic hydrogen carriers (LOHC),[10] for which hydrogen absorption and release occur well above room temperature and that faces challenges due to energy consumption, evaporative product selectivity,[10] and safety concerns due to the flammability of carrier molecules at such temperatures.

Here, we demonstrate and characterize an aqueous hydrogen storage method using an inexpensive organic molecule, anthraquinone disulfonate (AQDS), dissolved in an acidic electrolyte, as the hydrogen carrier. This method allows reversible hydrogen storage and release at ambient temperature and pressure using a voltage swing of <1 V, rather than a temperature or pressure swing. Furthermore, we demonstrate that AQDS can also be used as a water splitting mediator: during electrolysis, the oxygen evolution reaction is coupled with AQDS storing hydrogen directly in its reduced form, H_2AQDS; later, oxidation of H_2AQDS can release hydrogen based on demand. While a recently reported AQDS-mediated fuel cell utilizes an electrochemical half-reaction of H_2AQDS oxidation paired with the oxygen reduction reaction (ORR),[13] our hydrogen storage system utilizes a half-reaction of AQDS with protons and involves hydrogen oxidation and evolution.[14]

The structure of the AQDS hydrogen storage cell is shown in Figure 1. A cation exchange membrane (CEM) was sandwiched between carbon paper and a gas diffusion electrode (GDE). In the hydrogen chamber, electrons were transferred by a hydrophobic GDE. The GDE surface in contact with the CEM was coated with a layer of catalyst (0.5 mg/cm^2 60% Pt/C) on hydrophobic carbon paper to promote the hydrogen oxidation reaction (HOR) during storage and the hydrogen evolution reaction (HER) during release. SEM micrographs of the Pt/C-coated electrode are shown in Figure S1. The catalytic layer was pressed against the CEM to form a zero-gap cell. AQDS solution was pumped through the electrolyte chamber from a reservoir, which was protected by flowing N_2 in its headspace. Humidified hydrogen gas was delivered through the GDE in the hydrogen chamber.

Hydrogen storage occurs via the following electrochemically reversible reactions:

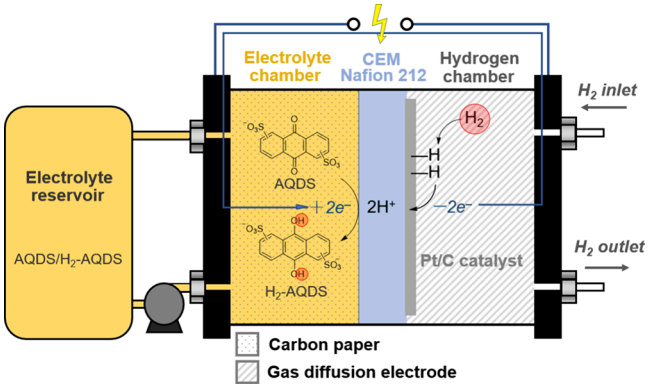

Figure 1. Hydrogen storage system schematic illustrating the storage mechanism.

$$H_2 \rightarrow 2H^+ + 2e^-$$

$$AQDS + 2H^+ + 2e^- \rightarrow H_2AQDS$$

In the cell, hydrogen gas flowing through the GDE was oxidized into protons. Simultaneously, AQDS was reduced to H_2AQDS through a proton-coupled electron transfer (PCET) process. When an opposite bias with respect to open circuit voltage (OCV) was applied to the cell, all of the processes could be reversed, and hydrogen gas was released at a controlled pressure. In the scope of this study, all hydrogen storage and release were performed under ambient pressure.

RESULTS AND DISCUSSION

Hydrogen absorption/release cycles were first demonstrated with 0.06 M 2,6-AQDS in 0.5 M H_2SO_4 as a working electrolyte (Figure 2). Figure 2a shows the cell potential ($E_{cell} = E_{H2} - E_{AQDS}$) vs capacity. The upper part of the figure shows the hydrogen storage behavior, while the lower part shows its release. The experimental charge storage capacity of 10 mL of 0.06 M AQDS solution in the reservoir was 35.5 mAh (vertical line in Figure 2a) at 4 mA/cm^2 cutoff current density, indicating that each AQDS molecule reacts with two electrons, which is consistent with the capacity reported by Chen et al.[15] The area-specific resistance (ASR) and the OCV of the 0.06 M cell vs state of charge (SOC) are shown in Figure 2b. High-frequency ASR obtained through electrochemical impedance spectroscopy (EIS) indicates that the ohmic resistance of the cell is approximately 0.6 Ω·cm^2 over the entire SOC range. Polarization ASR from linear sweep voltammetry (LSV), which adds to the contributions from polarization bias, reaction kinetics, charge transfer, and mass transport, is about 0.5−1.0 Ω·cm^2 higher than the ohmic resistance. LSVs of cells with different electrolyte concentrations exhibited similar behavior (Figure S2), indicating that the mass transport of AQDS is not limiting cell performance. According to cyclic voltammetry (CV), H_2 mass transport is also not a significant contributor to rate limitation when the current density is less than 250 mA/cm^2 under ambient pressure (Figure S3). Therefore, during cell operation with a current density lower than 200 mA/cm^2, the energy cost of the hydrogen storage/releasing cycle is mainly caused by ohmic resistance and polarization bias in the electrochemical cell.[16]

Figure 2c shows the long-term behavior of the cell over 5 days, exhibiting a capacity fade rate at 0.17%/day. The capacity fade is believed to be caused by molecule degradation. Jing et

https://doi.org/10.1021/acsaem.4c01233
ACS Appl. Energy Mater. XXXX, XXX, XXX−XXX

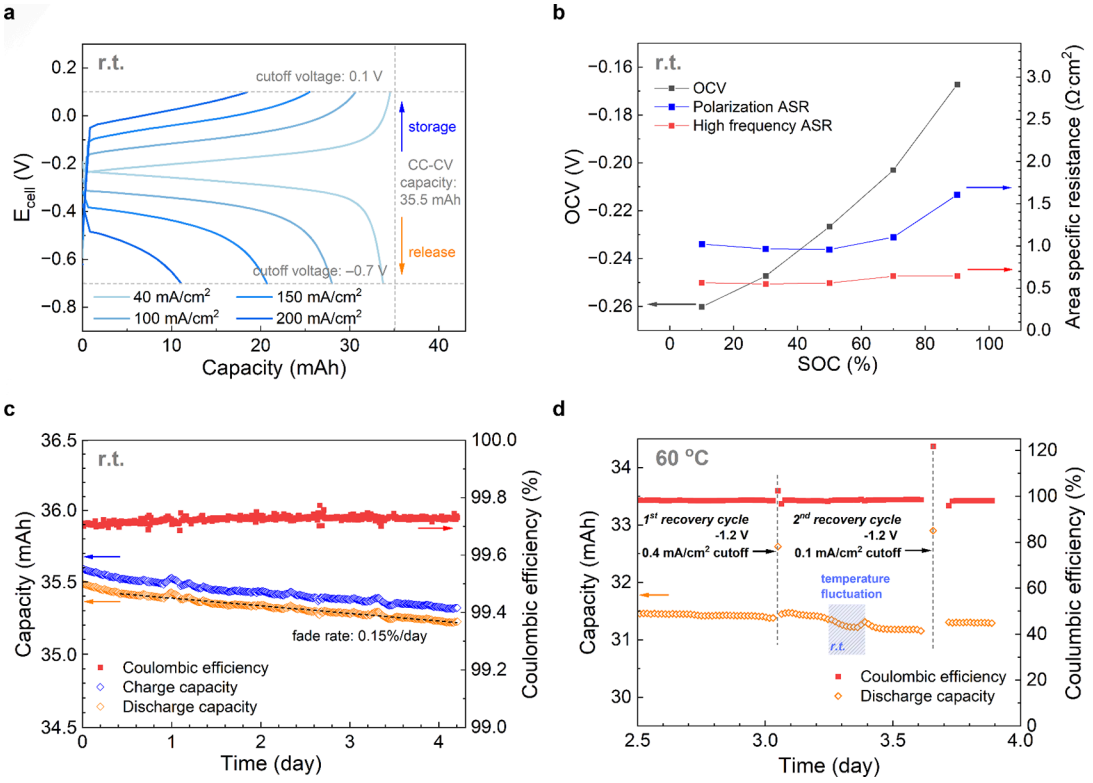

Figure 2. Cell performance with 10 mL of 0.06 M 2,6-AQDS as the electrolyte at room temperature, unless otherwise identified. (a) Cell potential vs capacity during the constant-current process at room temperature (r.t.); (b) OCV and area-specific resistance vs SOC; (c) long-duration CC−CV[18] cycling performance. A fade rate of 0.15%/day is calculated based on first-order reaction fitting from 0.4 to 4.2 days; (d) fade recovery at 3.05 and 3.55 days in a different cell with an initial discharge capacity of 32.3 mAh, subjected to constant-current followed by constant-voltage (CC−CV) cycling at 60 °C.

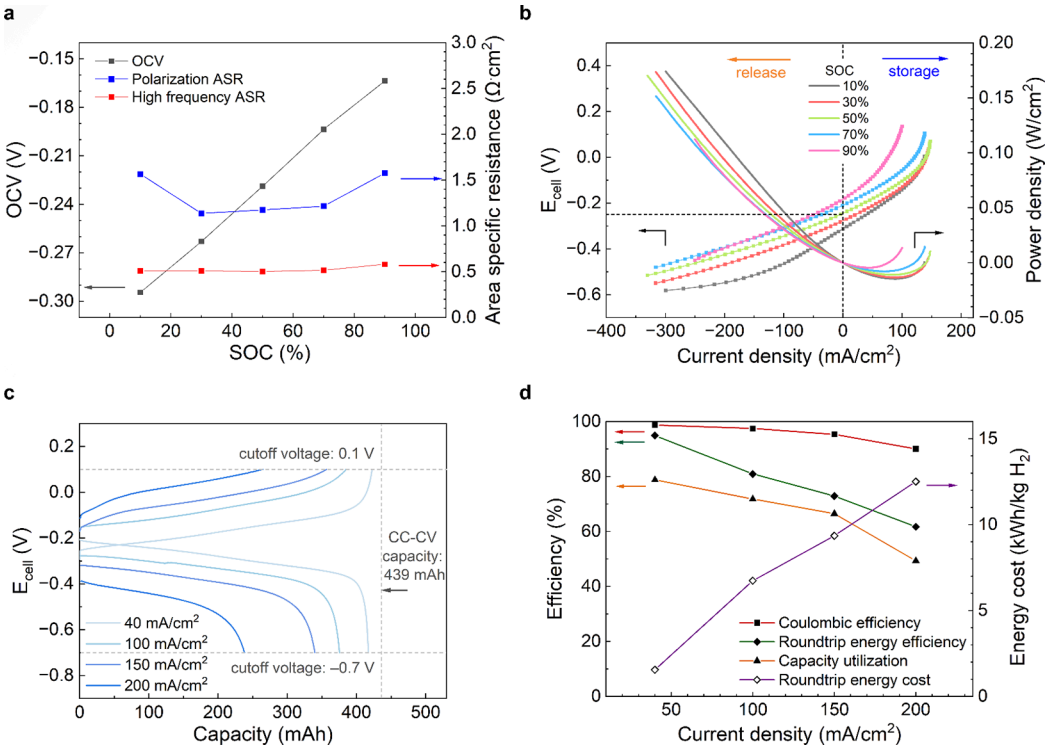

Figure 3. Cell performance with 1 M 2,6-AQDS as the electrolyte. (a) OCV and area-specific resistance vs SOC; (b) hydrogen release/storage LSV and power curve at various SOC; (c) cell potential vs capacity during galvanostatic charge and discharge; (d) capacity utilization, Coulombic efficiency, round-trip energy efficiency (HHV basis), and round-trip energy cost of hydrogen storage vs current density.

https://doi.org/10.1021/acsaem.4c01233
ACS Appl. Energy Mater. XXXX, XXX, XXX−XXX

al.[17] showed that degraded anthraquinone (in the form of anthrone and its dimer) can be electrochemically oxidized back to redox-active anthraquinone *in situ* in a flow battery. We employed a similar oxidative voltage excursion to investigate to what extent we could recover loss of AQDS capacity in another hydrogen storage cell (Figure 2d). In the recovery cycles at days 3.05 and 3.65, we polarized the electrolyte side at 1.2 V, instead of 0.7 V as in normal cycles, with respect to the hydrogen side. The two recovery attempts recovered 7.1 and 12.0% of loss capacities, respectively. Note that the cutoff current density was different in the two cases. Interestingly, we also observed that a large temperature fluctuation from 60 °C to room temperature and back can also affect capacity. The Coulombic efficiency away from the recovery events averaged 98.5%.

To test the robustness of the system with a higher electrolyte concentration, we used 1 M AQDS as a storage electrolyte. The cell showed a slower fade rate of only 0.072%/day in a cycling experiment lasting 1.7 days (Figure S8). The OCV, high-frequency ASR, and polarization ASR vs SOC are shown in Figure 3a. Although the high-frequency resistance is very close to that of the 0.06 M cell, the polarization resistance is somewhat higher. Increased resistance might be a result of more sluggish mass transport due to higher viscosity from higher concentrations.

Figure 3b shows the LSV and power curve of a 1 M AQDS cell under various SOCs. In the LSV curve set, we observe a limiting current density that is independent of SOC at low and intermediate SOC (0−70%) but that drops significantly at 90% SOC. Our interpretation of these observations is that in the 0−70% SOC range, the AQDS concentration is not affecting the limiting current, and the reaction is likely limited by the HOR on the other side of the cell. As the SOC goes up to 90%, the rate-limiting factor changes from HOR to AQDS mass transport. The power curve indicates that the electrolyte can spontaneously absorb hydrogen at a rate of up to ∼150 mA/cm^2 at 70% and below, whereas spontaneous hydrogen absorption reaches only ∼80 mA/cm^2 in the case of 90% SOC. Note that this spontaneity originates from the thermodynamically downhill reaction between AQDS and H_2, as evidenced by the negative storage power.

The cell behavior under galvanostatic conditions at various current densities is shown in Figure 3c,d. The capacity utilization, Coulombic efficiency, and round-trip energy efficiency dropped monotonically as current density increased. Round-trip energy cost was obtained by integrating the voltage−capacity behavior during a hydrogen absorption/release cycle, and the round-trip energy efficiency was reckoned as the difference between unity and the ratio of the energy cost to the HHV of hydrogen (39.8 kWh/kgH_2). When a 1 M AQDS solution served as the electrolyte and the current ranged from 40 to 200 mA/cm^2, the round-trip energy cost ranged from 1.6 to 12.5 kWh/kgH_2 and the round-trip energy efficiency ranged from 95 to 62%. Based on the linearity of the energy cost vs current density curve, it is apparent that the energy cost and capacity utilization penalties arise mainly from the cell resistance.

To explore the ability to reach a higher hydrogen storage density, we investigated the mixing of AQDS isomers at elevated temperature. We reached an ∼2.48 gH_2/L storage density (Figure S9) in 1.24 M AQDS solution. Furthermore, we reached an ∼2 M AQDS saturation concentration by simply mixing 2,6- and 2,7-AQDS at 35.7 °C. We expect that this concentration can be extended when the temperature is further increased or more isomers or other similar molecules are added to the solution. To confirm the Faradaic efficiency of the hydrogen absorption/release cycle (doubled moles of absorbed or released H_2 divided by the moles of electrons delivered) with mixed AQDS species, we performed a 0.9 day continuous charge/discharge run with 10× diluted saturated mixture solution (Figure S10). With the cell potential swing from −0.7 to 0.1 V, the cell went on CC−CV cycles with the current density set to 100 mA/cm^2 and cutoff current density of 4 mA/cm^2. During the electrochemical test, the amount of hydrogen captured and released was evaluated using the experimental setup shown in Figure 4a. After dry hydrogen

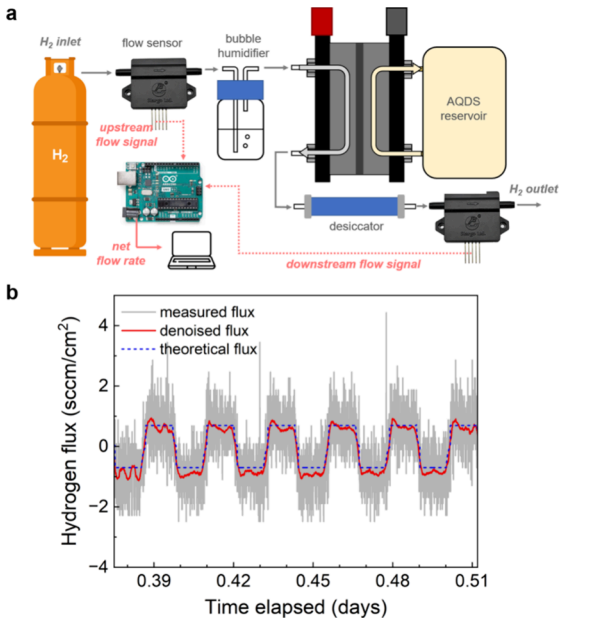

Figure 4. Cell performance with 0.2 M mixed 2,6- and 2,7-AQDS electrolytes at room temperature. (a) Schematic of the flow sensor setup; (b) measured, denoised, and theoretical flux over cycles 15−20 for 38 cycles spanning 0.9 days of continuous CC−CV charge/discharge at 100 mA/cm^2 with a cutoff current density of 4 mA/cm^2.

inlet flow went through an upstream flow sensor, hydrogen was humidified to maintain the ion conductivity of the CEM. Hydrogen storage and release took place in the cell, and the outlet gas stream was sent through a desiccator before entering the downstream flow sensor. Flow sensor signals were converted into flow rate after calibration (Figure S10). The changes in the flow rate over time were used to evaluate the amount of absorbed or released hydrogen.

In Figure 4b, we show the 15th through 20th cycles. Experimental and theoretical net hydrogen fluxes are plotted against time elapsed. The gray line shows the detected net flux, and the orange line shows the filtered signal by a 50-point moving average. The blue line is the theoretical hydrogen flux calculated from the current. From a comparison of the theoretical and filtered signal, we conclude that the Faradaic efficiency of hydrogen storage/release with mixed AQDS is close to 100%, confirming the high conversion and selectivity of this method. Note that because the AQDS reservoir was exposed to air and protected only by the overhead flow of N_2, the oxidation of H_2AQDS by oxygen resulted in net hydrogen

https://doi.org/10.1021/acsaem.4c01233
ACS Appl. Energy Mater. XXXX, XXX, XXX−XXX

consumption and led to a marginally lower release than absorption.

This aqueous electrochemical hydrogen storage cell, featuring reversible absorption and release, can be used in other energy and environmental applications.[13,19−21] One such application could be pressurized hydrogen-equivalent solution transfer that, coupled with water splitting (Figure 5), avoids

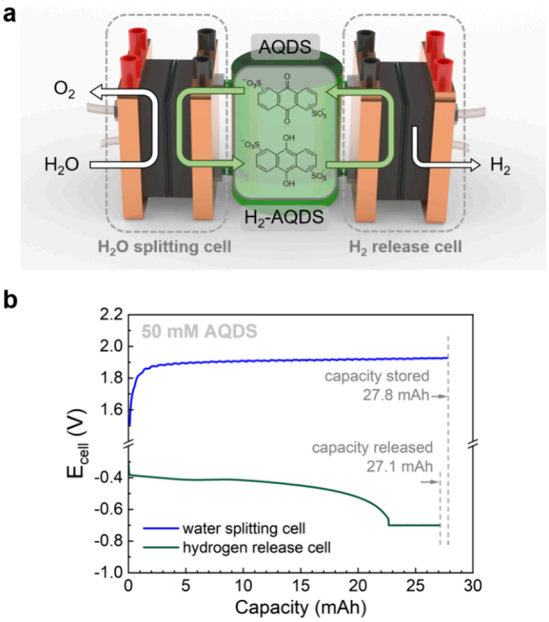

Figure 5. Temporally decoupled water splitting using the H_2O-(H_2SO_4)||AQDS(H_2SO_4) and H_2AQDS(H_2SO_4)||H_2 cell. (a) Cell structure: the red side serves as the working electrode, and the black side serves as the counter/reference electrode in both cells; (b) cell voltage vs capacity curve overlaid for the two cells.

issues brought by high diffusivity and reactivity of pressurized gaseous hydrogen, such as hydrogen leakage and metal embrittlement.[22] Another application would be decoupling the time hydrogen is released from the time when electrical energy must be put into water splitting. Such decoupling would make it possible to use variable renewable energy to split the water but release hydrogen whenever it is needed, *i.e.*, it can function as an electricity intermittency buffer to facilitate hydrogen production. As an example, this concept was demonstrated through a two-cell setup in which the AQDS electrolyte reservoir was shared by both cells (Figure 5a). The AQDS reservoir in the demonstrated system could be implemented as a pipeline that can transfer electrochemically active hydrogen in industrial designs. Also, the transferred hydrogen density can be tuned by the concentration of AQDS in the reservoir, with 1 M AQDS transferring 22.4 bar-equivalent H_2. In the demonstration, we used 50 mM AQDS as the reservoir electrolyte. The first cell (H_2O(H_2SO_4)||AQDS-(H_2SO_4)) takes in water, supported with 0.5 M sulfuric acid, and performs the oxygen evolution reaction (OER), while on the other side of the cell, AQDS is reduced to H_2AQDS. The OER onset cell potential in this AQDS-aided cell was ∼1.4 V, and the OER was performed galvanostatically at 40 mA/cm^2 (Figure 5b). Then, we switched the potentiostat to the H_2AQDS(H_2SO_4)||H_2 cell, sharing the AQDS reservoir with the previous cell as the electrolyte chamber. The HER was performed galvanostatically at 100 mA/cm^2 with a cutoff current density of 4 mA/cm^2, with the hydrogen side subjected to negative polarization. A total charge of 27.8 mAh was transferred to AQDS in the reservoir during the OER, and 27.1 mAh was released subsequently in the second cell through the HER, showing 97.5% water splitting-coupled hydrogen transfer efficiency. Additionally, by simply reversing the operation on the H_2 release cell to perform HOR and on the H_2O splitting cell to perform ORR, this system can readily become an AQDS-mediated H_2 fuel cell (Figure S13).

CONCLUSIONS

As shown in Figure 3d, the round-trip energy cost of storage and release ranges from 1.6 to 12.5 kWh/kgH_2 as the current density ranges from 40 to 200 mA/cm^2. The round-trip energy cost at 200 mA/cm^2 is comparable to that consumed in industrialized LOHC techniques,[23] whereas the 40 mA/cm^2 case is significantly lower. Because cell resistance is the primary cause of voltage loss, better energy efficiency could be achieved by using membranes with lower resistance. The capacity fade rate of approximately 0.07%/day might possibly decrease through previously demonstrated capacity recovery techniques. Another application for this redox chemistry, water splitting-coupled hydrogen transfer, was demonstrated through a dual-cell setup. Utilizing a solution of mixed 2,6- and 2,7-AQDS at elevated temperature, we raised the hydrogen storage density to 1.24 M. The hydrogen storage density at this concentration is equivalent to that of compressed $H_2(g)$ at only 30.7 bar, and it is unclear how high the storage density can be pushed in aqueous flow cells. This suggests a potential research area focused on achieving higher storage density through the use of smaller or mixed PCET-active molecules, which could enhance solubility. It is worth noting that, unlike mechanical compressors, an electrochemical cell can readily accept and release high-pressure hydrogen without major round-trip efficiency penalties from the pressurization.[24] Such cells can be particularly flexible with regard to pressure when the counter electrolyte is an incompressible liquid. In the scope of this study, however, increased viscosity of a highly concentrated AQDS solution might cause sluggish mass transport and heavy pump duty. Nevertheless, it is also unclear how developing stationary storage markets will value safety and efficiency compared with storage density.

Aqueous low-voltage electrochemical hydrogen storage through proton-coupled electron transfer without a swing in temperature or pressure provides a new method for stationary storage of massive amounts of hydrogen in a nonexplosive, fireproof medium. This approach appears attractive in settings where the storage density can be sacrificed for increased safety. The introduction of PCET-active organic molecules can reduce cost and material availability constraints and opens a wide design space for chemical hydrogen storage materials.

EXPERIMENTAL METHODS

All reagents were purchased from Sigma-Aldrich or Alfa Aesar and used as received, unless otherwise stated.

Flow Cell Setup. Flow battery experiments were constructed with cell hardware from Fuel Cell Tech (Albuquerque, NM) assembled into a zero-gap flow cell configuration. Pyrosealed POCO graphite flow plates with serpentine flow patterns were used for both electrodes. Each electrode comprised a 5 cm^2 geometric surface area, and the current was collected with two copper current collectors. The cell was assembled with two Viton (PVDF) gaskets for sealing purposes and a Nafion NR212 membrane, pretreated by soaking in DI water for 2 h in between. Four sheets of Sigracet 39 AA carbon paper

https://doi.org/10.1021/acsaem.4c01233
ACS Appl. Energy Mater. XXXX, XXX, XXX−XXX

electrodes (thickness 280 μm) were used in the electrolyte chamber. Three sheets of PTFE-treated TGP-H-60 Toray carbon paper (Alfa Aesar, thickness 200 μm) electrodes and one sheet of 0.5 mg/cm^2 60% Pt−C catalyst-coated PTFE-treated Vulcan carbon paper (Fuel Cell Tech, thickness 215 μm) were used in the hydrogen chamber. All electrodes were baked at 400 °C for 8 h. The catalyst layer was in contact with the CEM to form the zero-gap configuration. The AQDS electrolyte (10 mL) was driven by a Masterflex L/C pump through the electrolyte chamber and controlled at 48 mL/min. All cells were cycled at room temperature, unless otherwise stated. All hydrogen flow was at ambient pressure and bubbled through water for humidification prior to entering the cell.

Electrochemical Measurements. All electrochemical measurements were performed with a Biologic SP-150e potentiostat and corresponding software. The hydrogen chamber current collector served as the working electrode, while the electrolyte chamber served as the reference. Potentiostatic, galvanostatic, and CC−CV experiments all had sample intervals of 3 s. We employed the CC−CV charging method in all long-term fade test experiments due to its higher tolerance for minor temperature fluctuations and pumping noise compared to CC[25] as well as its ability to ensure full utilization of all available active materials. CVs and LSVs were performed at 20 and 100 mV/s, respectively.

Flow Measurements. Flow measurements were performed using two Siargo FS4001-100-V-A flow sensors to monitor the upstream (serial: B010459) and downstream (serial: B010460) hydrogen flow. Flow sensor data were transmitted to an Arduino UNO board and were then extracted using Python 3.7.6. All flow was dried with in-line drierite (Cole-Parmer) prior to entering the flow sensor.

AQDS Preparation. 9,10-Anthraquinone-2,6-disulfonic acid disodium salt (41.2 g, 0.1 mol) was dissolved in 100 mL of DI water.[26] Then, the solution was flushed through an acid-pretreated (1 M sulfuric acid) cation exchange resin (Amberlyst 15, Thermo Fisher Scientific) column. The column was washed with DI water, and the eluent with ion-exchanged solution was collected. The ion exchange process was repeated three times. The solution was dried and yielded 9,10-anthraquinone-2,6-disulfonic acid as a dark brown solid. Note that the sulfide groups were inclined to entrain water molecules within the crystalline structure, so the concentration of AQDS in the yielded solid might be diluted by up to ∼20%.

Hydrogen Flux Processing. Hydrogen flux was monitored by Siargo FS4001-100-V-A flow sensors. Both the inlet sensor (serial: B010459) and outlet sensor (serial: B010460) were calibrated by using dry hydrogen gas. The flow readings were calculated from the calibration curve (Figure S10). Denoised flow values were calculated by averaging 25 data points before and after each data point.

$H_2O(H_2SO_4)$||AQDS(H_2SO_4) Cell Setup for Water Splitting-Coupled Hydrogen Storage. All cell setups were identical to the section described in the Flow Cell Setup section except on the anode (OER) side, four sheets of baked Sigracet 39 AA carbon paper electrodes with one sheet of them coated with 5 mg/cm^2 20% Ir−C. The Ir−C-coated side has direct contact with the Nafion NR212 membrane.

■ ASSOCIATED CONTENT

Supporting Information

The Supporting Information is available free of charge at https://pubs.acs.org/doi/10.1021/acsaem.4c01233.

Experimental description; preparation of active chemicals; characterization of electrode, cell, and membrane performances; and flow sensor standard curve (PDF)

■ AUTHOR INFORMATION

Corresponding Author

Michael J. Aziz − *Harvard John A. Paulson School of Engineering and Applied Sciences, Cambridge, Massachusetts 02138, United States;* orcid.org/0000-0001-9657-9456; Email: maziz@harvard.edu

Authors

Taobo Wang − *Harvard John A. Paulson School of Engineering and Applied Sciences, Cambridge, Massachusetts 02138, United States;* orcid.org/0000-0002-4286-6414

Dawei Xi − *Harvard John A. Paulson School of Engineering and Applied Sciences, Cambridge, Massachusetts 02138, United States;* orcid.org/0000-0002-5412-3474

Complete contact information is available at: https://pubs.acs.org/10.1021/acsaem.4c01233

Author Contributions

†T.W. and D.X. contributed equally to this work.

Notes

The authors declare no competing financial interest.

■ ACKNOWLEDGMENTS

This research was supported by the Harvard John A. Paulson School of Engineering and Applied Sciences.

■ REFERENCES

(1) *Hydrogen and Fuel Cell Technologies Office* https://www.energy.gov/eere/fuelcells/hydrogen-and-fuel-cell-technologies-office, accessed Nov 30.

(2) *"Hydrogen Hurdles: A Deadly Blast Hampers South Korea's Big Fuel Cell Car Bet,"* https://www.reuters.com/article/us-autos-hydrogen-southkorea-insight/hydrogen-hurdles-a-deadly-blast-hampers-south-koreas-big-fuel-cell-car-bet-idUSKBN1W936A/, accessed Nov 18.

(3) *Lessons Learned from a Hydrogen Explosion* https://www.powermag.com/lessons-learned-from-a-hydrogen-explosion/, accessed 2023.

(4) *Hydrogen Cylinder Transport Accident Results in Explosion* https://h2tools.org/lessons/hydrogen-cylinder-transport-accident-results-explosion accessed Nov 18.

(5) Usman, M. R. Hydrogen Storage Methods: Review and Current Status. *Renewable & sustainable energy reviews* **2022**, *167*, No. 112743.

(6) Barthelemy, H.; Weber, M.; Barbier, F. Hydrogen Storage: Recent Improvements and Industrial Perspectives. *International journal of hydrogen energy* **2017**, *42*, 7254.

(7) Jensen, J. O.; Vestbø, A. P.; Li, Q.; Bjerrum, N. J. The Energy Efficiency of Onboard Hydrogen Storage. *J. Alloys Compounds* **2007**, *446*, 723.

(8) Zhang, F.; Zhao, P.; Niu, M.; Maddy, J. The Survey of Key Technologies in Hydrogen Energy Storage. *International journal of hydrogen energy* **2016**, *41*, 14535.

(9) Chen, Z.; Kirlikovali, K. O.; Idrees, K. B.; Wasson, M. C.; Farha, O. K. Porous Materials for Hydrogen Storage. *Chem.* **2022**, *8*, 693.

(10) Rao, P. C.; Yoon, M. Potential Liquid-Organic Hydrogen Carrier (Lohc) Systems: A Review on Recent Progress. *Energies* **2020**, *13*, 6040.

(11) Chen, Z.; Li, P.; Anderson, R.; Wang, X.; Zhang, X.; Robison, L.; Redfern, L. R.; Moribe, S.; Islamoglu, T.; Gomez-Gualdron, D. A.; Yildirim, T.; Stoddart, J. F.; Farha, O. K. Balancing Volumetric and Gravimetric Uptake in Highly Porous Materials for Clean Energy. *Science* **2020**, *368*, 297.

(12) Ren, J.; Musyoka, N. M.; Langmi, H. W.; Mathe, M.; Liao, S. Current Research Trends and Perspectives on Materials-Based Hydrogen Storage Solutions: A Critical Review. *International journal of hydrogen energy* **2017**, *42*, 289.

(13) Yurko, Y.; Elbaz, L. Direct Quinone Fuel Cells. *J. Am. Chem. Soc.* **2023**, *145*, 2653.

(14) Wang, T.; Xi, D.; Aziz, M.J. *"Low Voltage Electrochemical Aqueous Hydrogen Storage"*, presented at the 243rd ECS Meeting, Boston, MA, 2023 (unpublished). .
(15) Chen, Q.; Eisenach, L.; Aziz, M. J. Cycling Analysis of a Quinone-Bromide Redox Flow Battery. *J. Electrochem. Soc.* **2016**, *163*, A5057.
(16) Robb, B.H.; George, T.Y.; Davis, C.M.; Tang, Z.; Fujimoto, C.H.; Aziz, M.J.; Marshak, M.P. "Sulfonated Diels-Alder Poly-(Phenylene) Membrane for Efficient Ion-Selective Transport in Aqueous Metalorganic and Organic Redox Flow Batteries", *J. Electrochem. Soc.* (**2023**). *170*, 030515.
(17) Jing, Y.; Zhao, E. W.; Goulet, M.-A.; Bahari, M.; Fell, E. M.; Jin, S.; Davoodi, A.; Jonsson, E.; Wu, M.; Grey, C. P.; Gordon, R. G.; Aziz, M. J. In Situ Electrochemical Recomposition of Decomposed Redox-Active Species in Aqueous Organic Flow Batteries. *Nature Chem.* **2022**, *14*, 1103.
(18) Yao, Y.; Lei, J.; Shi, Y.; Ai, F.; Lu, Y.-C. Assessment Methods and Performance Metrics for Redox Flow Batteries. *Nature energy* **2021**, *6*, 582.
(19) Perry, M. L. Electrochemically-Rechargeable Liquids in Highly Flexible Energy Storage Systems. *ECS Trans.* **2021**, *104*, 23.
(20) Rausch, B.; Symes, M. D.; Cronin, L. A Bio-Inspired, Small Molecule Electron-Coupled-Proton Buffer for Decoupling the Half-Reactions of Electrolytic Water Splitting. *J. Am. Chem. Soc.* **2013**, *135*, 13656.
(21) Kirkaldy, N.; Chisholm, G.; Chen, J.-J.; Cronin, L. A Practical, Organic-Mediated, Hybrid Electrolyser That Decouples Hydrogen Production at High Current Densities. *Chemical science (Cambridge)* **2018**, *9*, 1621.
(22) https://www.exponent.com/article/can-your-natural-gas-pipelines-handle-hydrogen-blends, *"Can. Your Natural Gas Pipelines Handle Hydrogen Blends?,"* accessed Dec 4.
(23) https://hydrogenious.net/what/#release-plants, *"Release Plants - Stationary Lohc Infrastructure – Supplying the Hydrogen Offtakers Right Where They Are,"* accessed March 23.
(24) Hancke, R.; Holm, T.; Ulleberg, Ø. The Case for High-Pressure Pem Water Electrolysis. *Energy conversion and management* **2022**, *261*, No. 115642.
(25) Fell, E. M.; Aziz, M. J. High-Throughput Electrochemical Characterization of Aqueous Organic Redox Flow Battery Active Material. *J. Electrochem. Soc.* **2023**, *170*, 100507.
(26) Metlay, A. S.; Chyi, B.; Yoon, Y.; Wycisk, R. J.; Pintauro, P. N.; Mallouk, T. E. Three-Chamber Design for Aqueous Acid–Base Redox Flow Batteries. *ACS energy letters* **2022**, *7*, 908.

https://doi.org/10.1021/acsaem.4c01233
ACS Appl. Energy Mater. XXXX, XXX, XXX–XXX

Supporting Information

Electrochemical hydrogen storage under ambient conditions in aqueous-soluble organics

Taobo Wang†, Dawei Xi†, and Michael J. Aziz*

Harvard John A. Paulson School of Engineering and Applied Sciences, Cambridge, Massachusetts 02138, United States.

† Authors with equal contribution

*Email: maziz@harvard.edu

Table of Contents

Characterization of hydrogen chamber electrode material

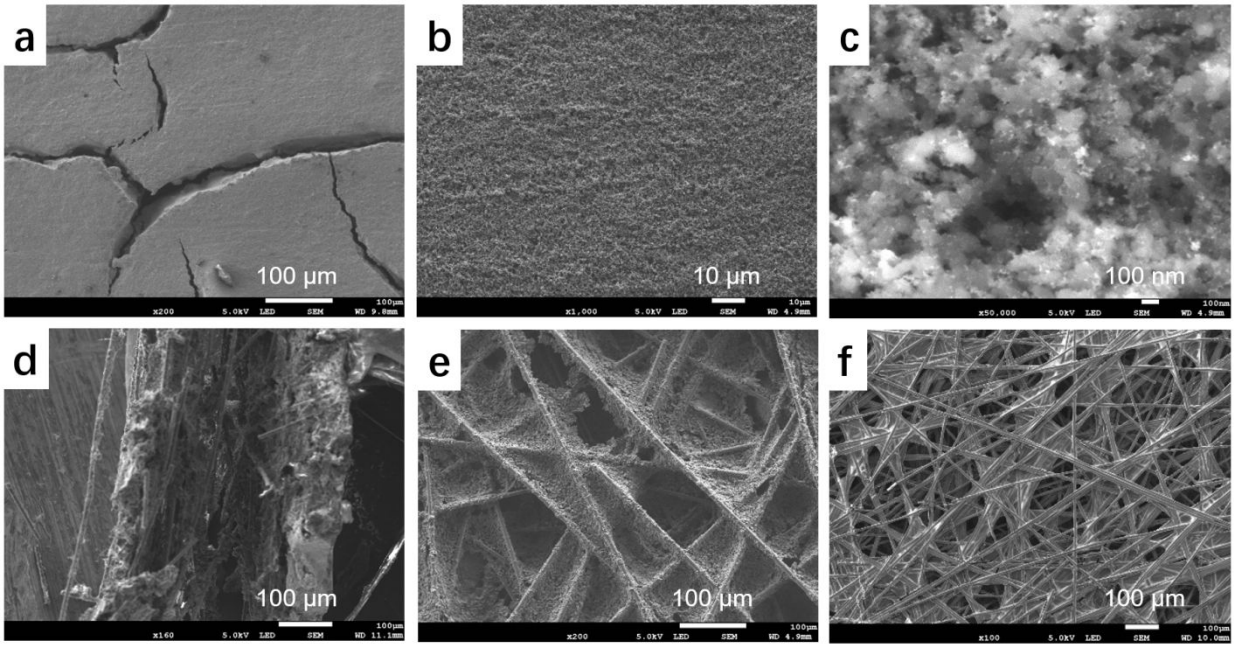

Figure S1. Hydrogen chamber electrode and catalyst layer structures by SEM. (a-c) 0.5 mg/cm^2 60% Pt/C heat-compressed GDE catalyst layer; (d) cross-sectional image of catalyst layer on carbon paper electrode; (e) backside of catalytic carbon paper electrode; (f) structure of PTFE treated TGP-H-60 Toray carbon paper electrode.

LSV curves for hydrogen absorption

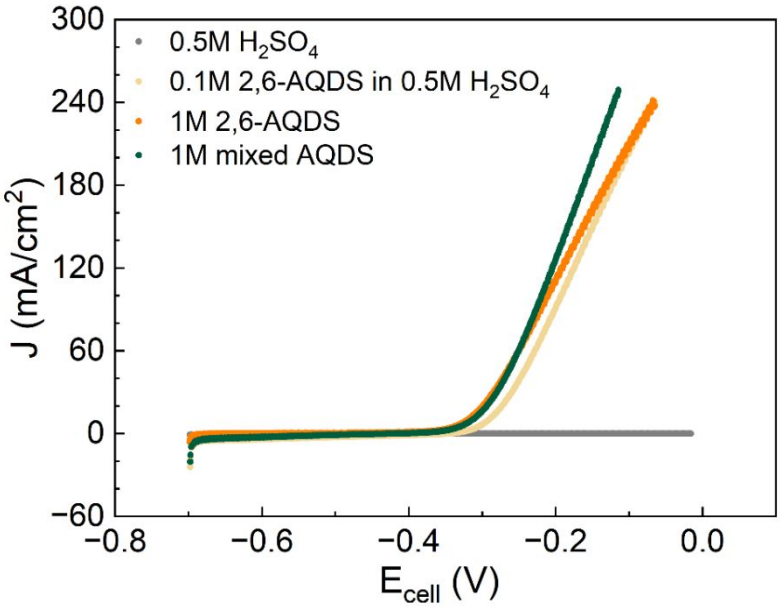

Figure S2. Linear sweep voltammetry of hydrogen absorption reaction with 0.5 M sulfuric acid, pH 1 0.1 M 2,6-AQDS, 1 M 2,6-AQDS, and 1 M mixed 2,6- and 2,7-AQDS in electrolyte chamber.

CV comparison of low and high H_2 flow rate

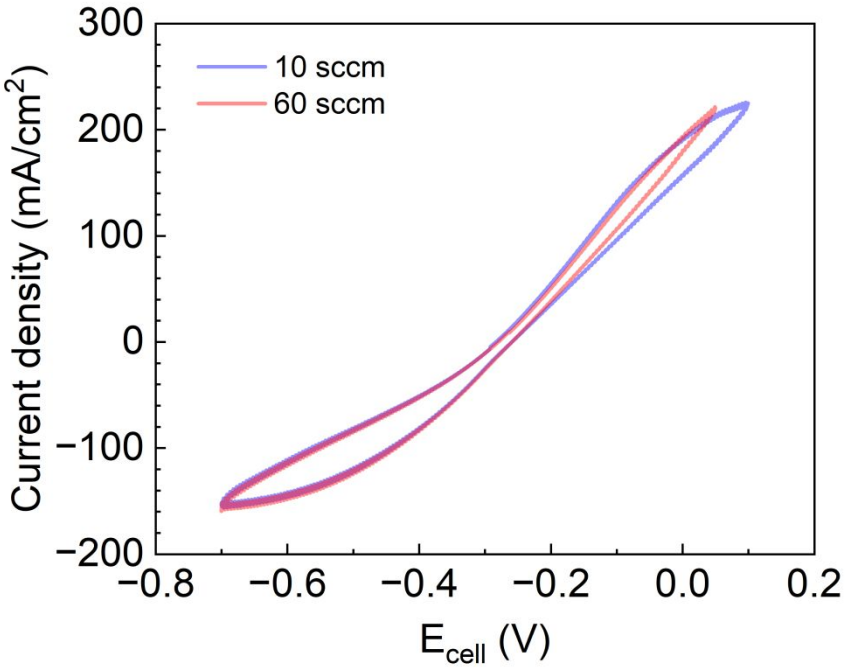

Figure S3. Cyclic voltammogram of 0.1 M AQDS cell with 10 and 60 standard cubic centimeters per minute (sccm) flow rate in a 5 cm^2 FCT cell described above in the experimental section. Note that $E_{cell} = E_{H2} - E_{AQDS}$. Positive current corresponds to hydrogen oxidation by AQDS.

Performance of Nafion NR212 with alternative pretreatments

We have compared the Nafion NR212 performance with two different pretreatments. Boiled pretreatment: NR212 was boiled in 0.5 M sulfuric acid for 1 h, then boiled in 3 wt.% hydrogen peroxide for 1 h, and finally boiled in DI water for 1 h. Soaked pretreatment: Nafion NR212 was soaked overnight in DI water at room temperature.

We pretreated the membrane with boiling 0.5 M H_2SO_4 and 3% H_2O_2 and obtained lower system resistance (Fig. S4) and lower energy cost. However, the boiled pretreatment loosens the membrane structure and aggravates molecular crossover (Fig. S5). Pretreatment with DI water yields significantly lower crossover rate[1]. The crossover not only affects the cell in long-term capacity performance, but the organic molecules that penetrate through the membrane can also poison the catalyst (Fig. S6). Thus, pretreating membranes with only room-temperature DI water to prevent the apparent crossover penalty is worth the sacrifice of slightly higher resistance and energy cost.

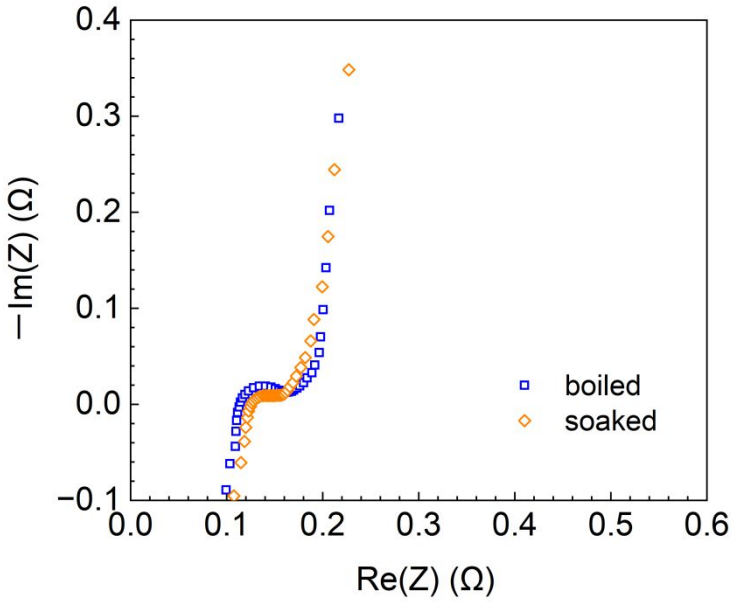

Figure S4. EIS data for Nafion NR212 with boiled (blue square) and soaked (orange diamond) pretreatments during hydrogen storage. Boiling pretreatment: boil NR 212 in 3 wt.% H_2O_2 and 0.5 M H_2SO_4 for 1 h, consecutively. Soak pretreatment: soak NR212 in DI water for 2 h in room temperature.

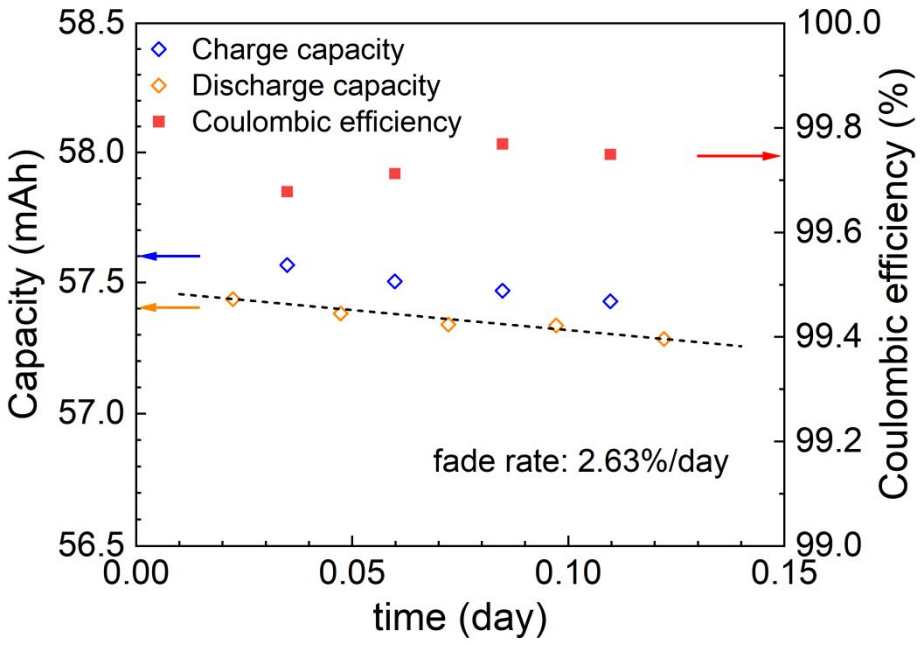

Figure S5. Cell performance with boil-pretreated membrane in 0.1 M 2,6-AQDS solution supports with 1.0 M sulfuric acid. Capacity and Coulombic efficiency were plotted against time for reversible hydrogen storage cycles with boil-pretreated NR212.

AQDS catalyst poisoning

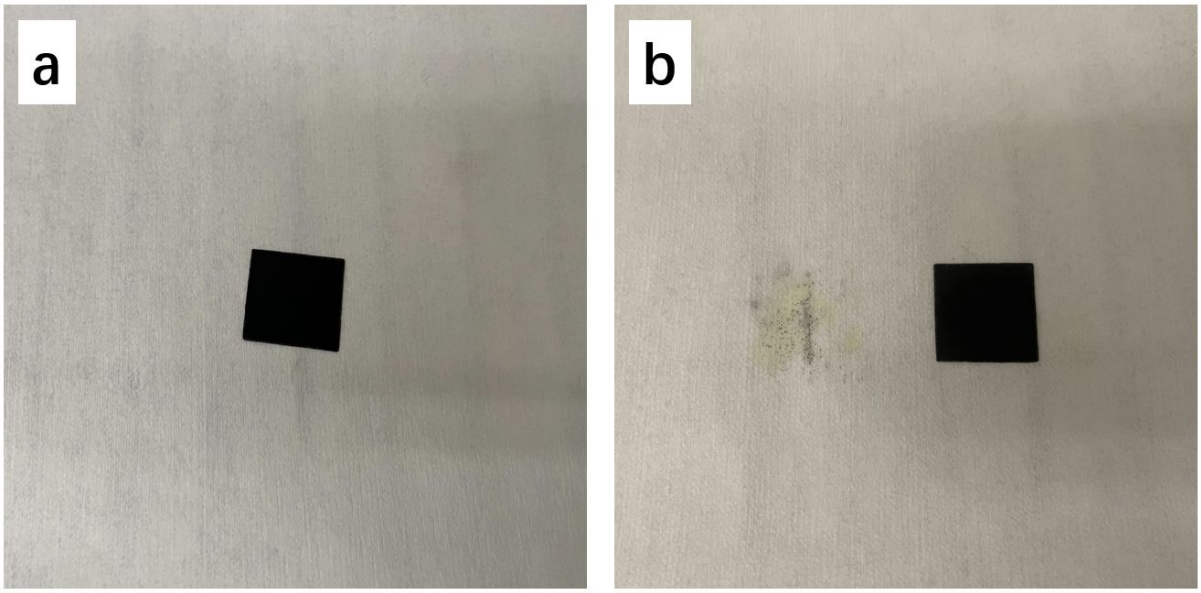

Figure S6. 60% Pt-C coated electrode with 0.5 mg/cm^2 loading. (a) pristine; (b) AQDS-poisoned electrode after 1 day cell test with 1 M AQDS and boiled Nafion® NR212.

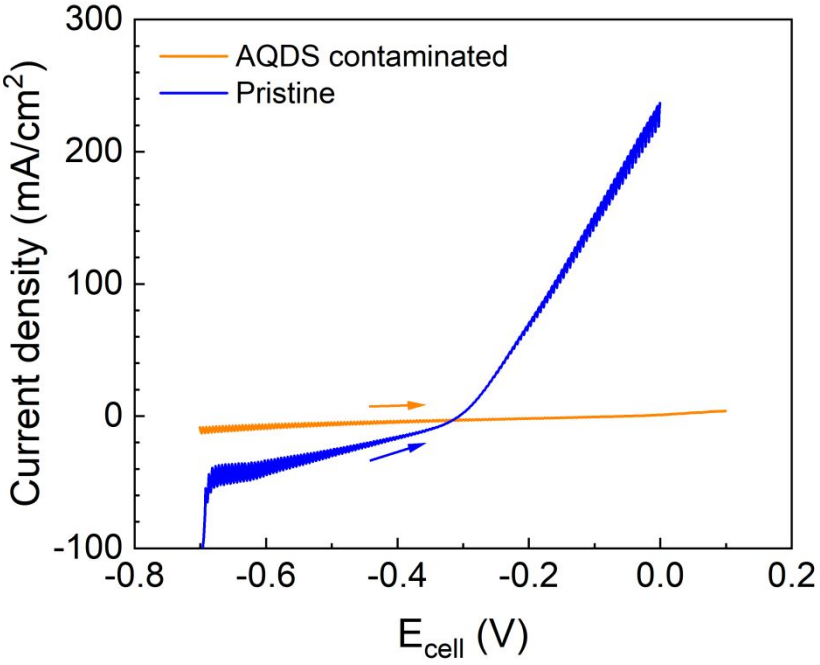

Figure S7. LSV of pristine (blue) and AQDS-poisoned (orange) 60% Pt-C coated electrode.

1 M AQDS fade test

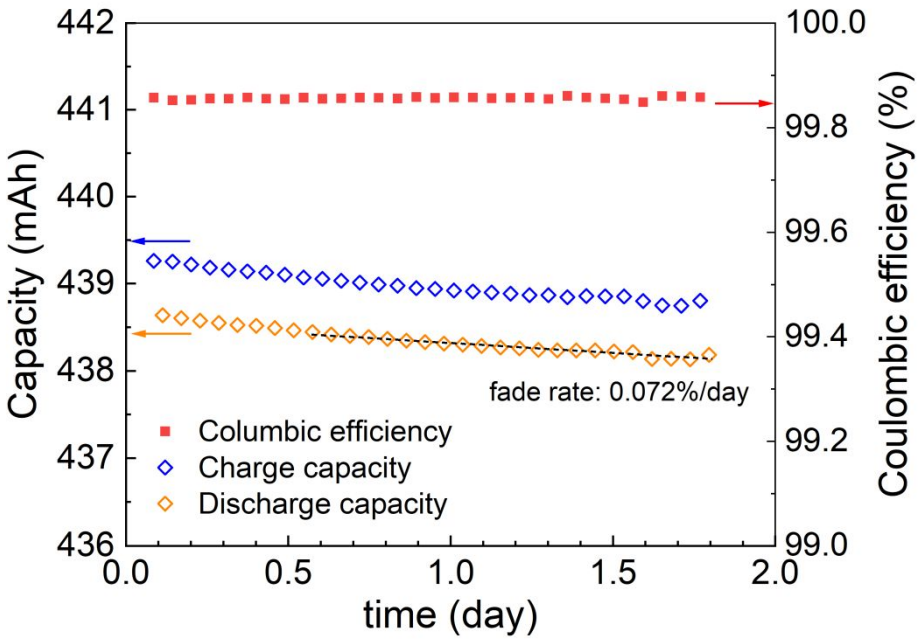

Figure S8. Capacity and Coulombic efficiency plot for reversible hydrogen storage cycles with 1 M 2,6-AQDS as storage electrolyte.

Mixed 2,6- and 2,7-AQDS cell performance

Hydrogen storage density was tested through series dilution of saturated solution of mixed 2,6- and 2,7-AQDS at 35.7 °C (Fig. S9). The saturation concentration is determined to be 2.07 M. The hydrogen storage density evaluated from coulometry was 0.04, 0.41, 0.81, and 1.24 M in 0.04, 0.41, 0.83, 1.24 M mixed AQDS electrolytes, respectively. The blue dashed line shows the theoretical hydrogen capacity curve, which is simply one molecule of H_2 per AQDS. A sudden drop of hydrogen storage density when AQDS concentration exceeded 1.5 M was accompanied with a notable increase in solution viscosity, indicating the formation of large molecule clusters, which could be either colloids or oversaturated reduced-form AQDS precipitates. Given the higher local density of molecules in clusters compared to dispersed solutions, each molecule in a cluster is expected to carry fewer charges. This is due to the instability caused by high local charge density in clusters. This could be a contributing factor to the incomplete absorption of hydrogen. Furthermore, the movement of large clusters might be restricted and thus limit the electron transfer process, leading to similar issues in the process. Also, the viscosity increase might also cause an increased pressure drop across the flow field, resulting a different flow pattern that potentially affects the accessed capacity.

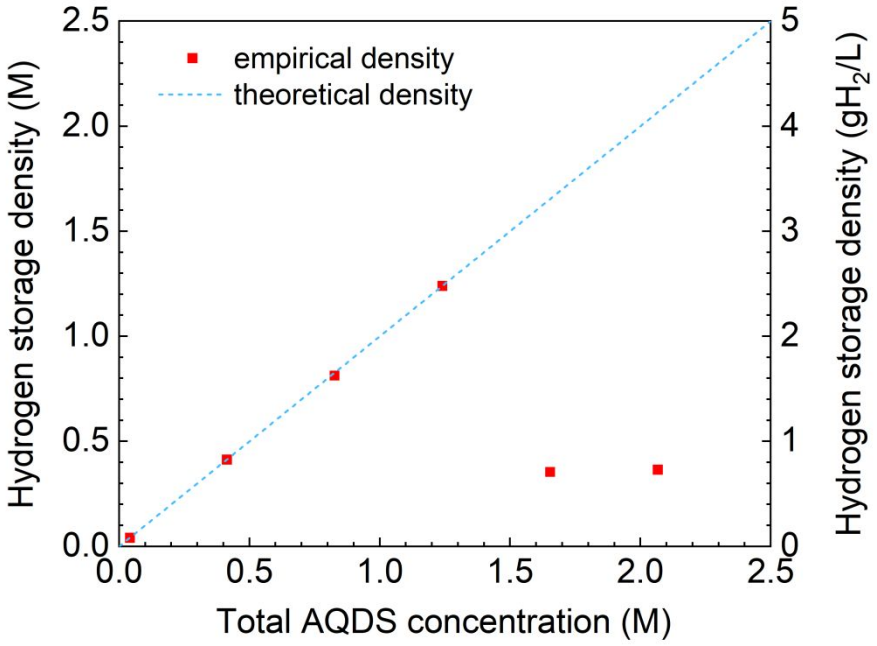

Figure S9. hydrogen storage density versus mixed AQDS concentration at 35.7°C.

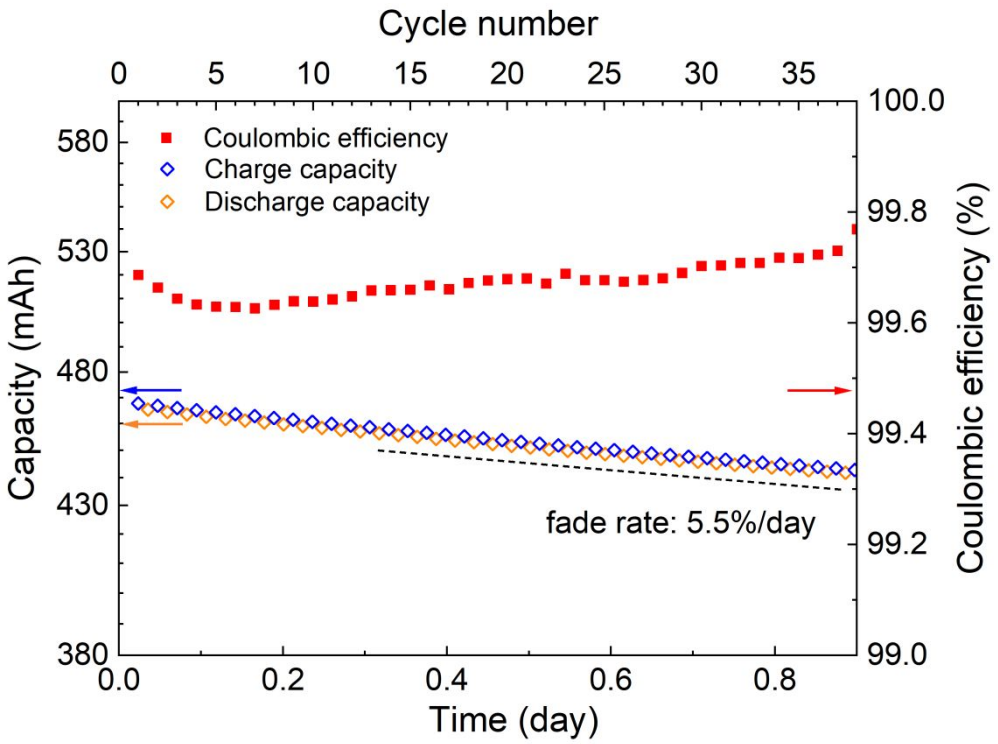

Figure S10. Cell performance with mixed 0.2 M equimolar 2,6- and 2,7-AQDS electrolyte showing fade and Coulombic efficiency from 0.3 to 0.9 day.

To increase the hydrogen storage density, we used mixed 2,6-AQDS and 2,7-AQDS to increase the solubility of overall quinone species. Figure S10 shows the cell performance from an electrolyte with 10× dilution from saturated solution at 35.7°C, whose coulombic efficiency is 99.7%.

Siargo® FS4001-100-V-A flow sensor standard curve

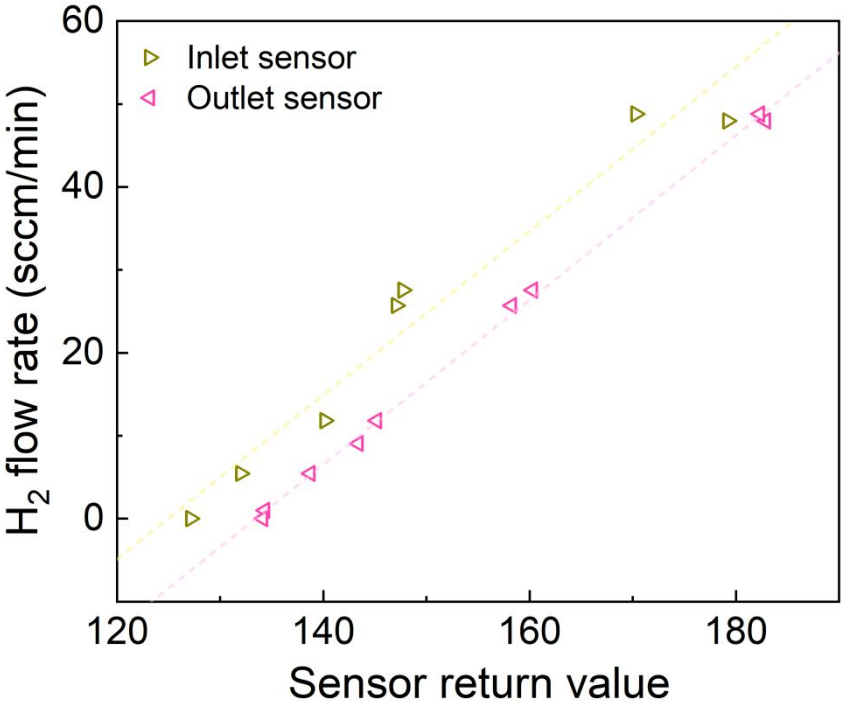

Figure S11. Siargo® FS4001-100-V-A flow sensor response curve under various hydrogen flow rates. Gray triangles correspond to data from inlet sensor (serial: B010459); pink triangles correspond to data from outlet sensor (serial: B010460).

Water splitting cell performance

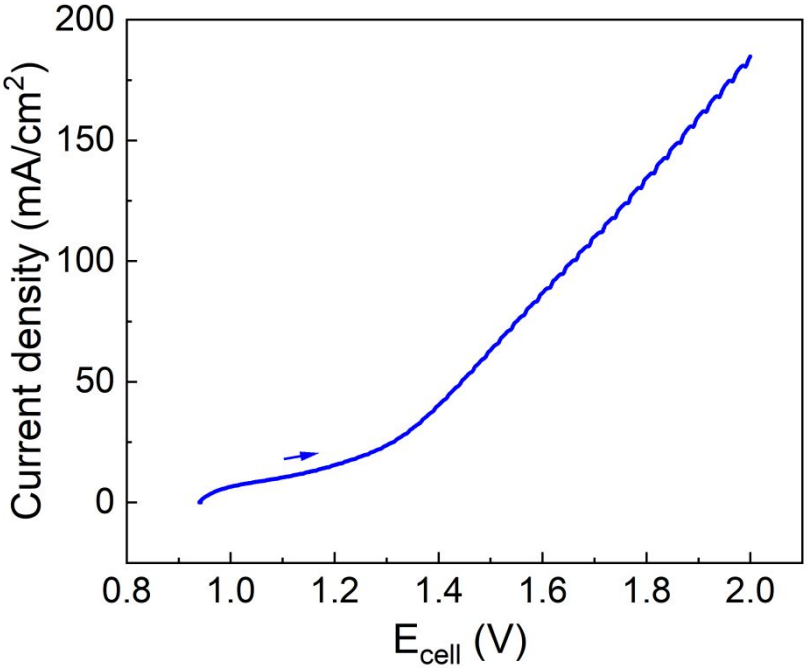

Figure S12. LSV of OER in $H_2O(H_2SO_4)$||$AQDS(H_2SO_4)$ cell against 1 M 2,6-AQDS. Detailed cell assembly was specified in *Experimental Methods* section.

Scheme of AQDS-mediated H_2 fuel cell

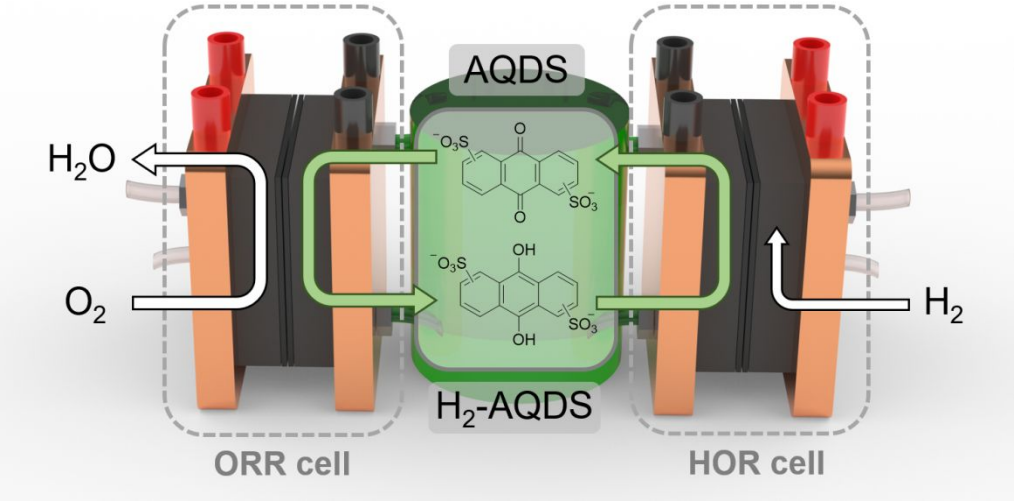

Figure S13. Cell structure for reverse operation of the system shown in Fig. 5a to perform as an AQDS-mediated H_2 fuel cell.

REFERENCES

(1) Robb, B. H.; George, T. Y.; Davis, C. M.; Tang, Z.; Fujimoto, C. H.; Aziz, M. J.; Marshak, M. P. Sulfonated Diels-Alder Poly(phenylene) Membrane for Efficient Ion-Selective Transport in Aqueous Metalorganic and Organic Redox Flow Batteries. *Journal of the Electrochemical Society* **2023**, *170* (030515). DOI: 10.1149/1945-7111/acbee6.